Detonation performance model calibration and validation of the HMX-based high explosive PBX 9501

C. Chiquete[1], S. I. Jackson[2], E. K. Anderson[1], M. Short[1], S. J. Voelkel[1] & V. H. Whitley[1]
[1] Los Alamos National Laboratory, Los Alamos, NM USA
[2] Texas A&M University, College Station, TX USA

1 Introduction

High explosives (HEs) are metastable compounds that are commonly used in engineering applications that require extremely high power. The accurate prediction of detonation propagation in the application geometry and the corresponding work done on adjacent materials is essential to the successful use of HEs within engineering applications. These two properties are collectively designated as the detonation performance for a given material. Due to their chemical complexity, empirically-derived detonation performance models for HEs are often calibrated to a series of experiments that utilize simplified geometries including confined and unconfined axisymmetric HE cylinders and/or rectangular cuboids ("slab"). In either case, experimental measurements provide steady-state propagation behavior and wall expansion rates when the explosive is confined (typically by a metal). The fundamental assumption is that detonation performance model parameterizations produced in one geometry, i.e. a Copper-confined cylindrical HE charge (CYLEX), can be used to accurately represent the HE behavior in more complex application geometries with a variety of confiner materials. Our main objective here is to generate confidence in this assumption by investigating the predictive capability of such a model for the ideal HMX-based PBX 9501[1].

To represent these experiments, we use an engineering methodology known as Programmed Burn (PB) to achieve greater numerical efficiency relative to traditional reactive flow methods which attempt to resolve the fine reaction zone (RZ) scales. These sub-scale methods require distinct front propagation and energy release methodologies and these have evolved in complexity over time. At its simplest, the propagation has been often treated with a simple requirement of a constant normal detonation velocity (i.e. the Chapman-Jouguet (CJ) detonation velocity) through the evolution of the front. In modern PB methods, the detonation propagation is instead modeled with Detonation Shock Dynamics (DSD) [1]. This methodology adds finite reaction zone effects which tend to reduce propagation speeds relative to the (planar) CJ limit. This model has been recently applied and validated to PBX 9501 propagation experiments [2]. Importantly, this work showed that the assumption of a constant propagation velocity implies significant timing errors in a unconfined 2D arc geometry, even for an conventional HE like PBX 9501.

[1] 95 wt.% cyclotetramethylene-tetranitramine (HMX) explosive crystals bonded with a binder mixture of 2.5 wt.% Estane and a 2.5 wt.% eutectic mixture of bis(2,2-dinitropropyl)acetal and bis(2,2-dinitropropyl) formal (BDNPA/BDNPF)

Correspondence to: chiquete@lanl.gov

Table 1: Shot details for the two confined experiments where ρ_0 is the HE initial density, T_{HE} refers to the thickness of the HE slab, d_{HE} is the HE cylinder diameter and D_0 is the measured phase velocity. The wall thickness for the cylindrical test should be considered an average as there are slight changes in concentricity of the Cu tube.

Shot #	Geometry	Confiner	ρ_0 (g/cm^3)	T_{HE} or d_{HE} (mm)	D_0 (mm/μs)	Wall thickness (mm)
8-1911	slab	Ta	1.834	10.03	8.782 ± 0.004	0.544-0.55
8-1932	slab	Cu	1.833	10.03	8.790 ± 0.004	1.02
8-1964	cylinder	Cu	1.837	25.410	8.825 ± 0.003	2.5235

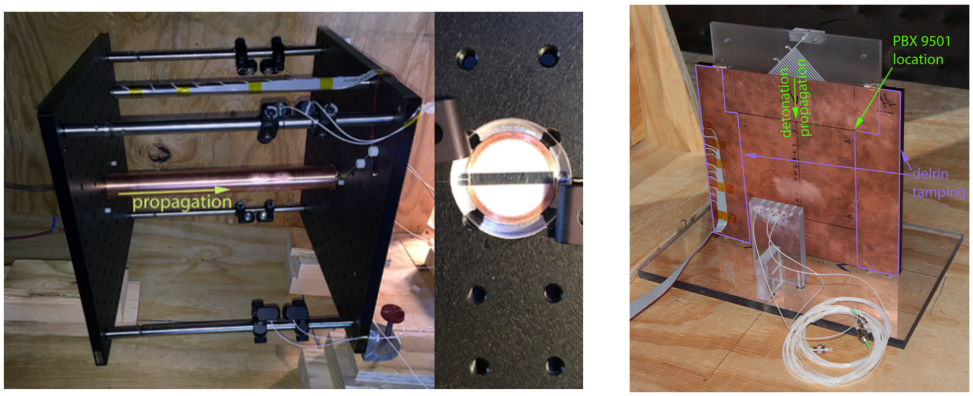

Figure 1: Left: Assembly photograph of the cylinder expansion test. A side view showing PDV probe locations is on the left, and a view of the streak camera window is on the right. Right: Assembly photograph of the confined slab test. The Cu confiner plates were larger than the PBX 9501 charge by 50.8 mm in all directions. The ends highlighted in pink were filled with Delrin tamping.

The calibration of a complete detonation performance model for PBX 9501 also requires an energy release methodology. For consistency with our DSD wave propagation [2], an energy release method is chosen that also takes the effects of divergently curved detonation waves into account. A previously-described calibration process for this model component utilizing successive hydrocode simulations of cylinder expansion tests is selected to refine the energy release and EOS parameters [3, 4, 5]. Though we have previously shown that the produced models can accurately represent the observed wall motion for a given calibration CYLEX test (for a variety of HEs), we have not specifically addressed the validation of these models. We do so here by calibrating our model in the CYLEX geometry and comparing its wall expansion predictions to confined slab geometry experiments with two different confining materials.

2 Experiments

The main test specifications for the two Copper (Cu) confined expansion tests (both a standard-scale CYLEX test and a confined slab geometry) and a third test using the slab geometry and Tantalum (Ta) confiner appears in Table 1. Note that the Cu-confined experiments have been partially described previously in [6] but more complete detail on the test assembly appears below. The cylinder expansion test in this study was assembled using 12 25.4 mm $\times$ 25.4 mm long PBX 9501 cylindrical pellets and a C101 copper tube. Prior to assembly, the copper tube was machined to nominal dimensions (25.4 mm ID, 30.48 mm OD, and 304.8 mm length). The tube was then honed to an ID between 0.01 mm and 0.025 mm greater than the diameter of the PBX 9501 cylinders. It was then annealed dead soft, and

measured at the PDV locations. At these locations, the post-annealing OD, ID, and concentricity of the bore relative to the outer surface were measured. Using these three measurements, the wall thickness at each PDV probe was inferred. The PBX 9501 pellets were coated with degassed, accelerated Sylgard 184 on all surfaces contacting either the confiner tube or adjacent pellets, and carefully placed in the tube to minimize any trapped air pockets. A line of 11 shorting wires was placed on the tube and measured before the assembly was placed on the stand shown in Fig. 1 (left). PDV probes were mounted along the rods connecting the stand end-plates, and 4 were positioned at 2/3 run distance, and another 4 at 3/4 run distance. All 8 PDV probes were aligned normal to the tube surface. In addition to shorting wires and PDV, a front shape was recorded using Cordin 132 streak camera to image the breakout surface of the shot along a center chord. The mirror destruction technique was used, with a vapor-deposited aluminum mirror on a PMMA window providing the reflective surface. An Argon flash was used to illuminate the mirror.

The slab expansion tests were conducted using a PBX 9501 charge that was 130 mm along the direction of detonation propagation, and 150 mm in the direction normal to propagation. The thickness of the charges was measured at 10 evenly spaced locations along the centerline, each PDV probe measurement location, and each of the corners. The thickness of the metal confining plates and the final thickness of the assembly were measured at the same locations so that the thickness of the glue layer could be inferred. The thicknesses reported in Table 1 are representative of measurement at the PDV probe locations. Accelerated Sylgard 184 was used to bond the confiner sheets to the PBX 9501 for 8-1911, while Angstrom Bond AB9320 was used for 8-1932. A photograph of 8-1932 is shown in Fig. 1 (right). The tests were instrumented with 11 shorting wires to measure detonation velocity. The wires were placed along a line parallel to detonation propagation and 25 mm from the centerline of the PBX 9501 slab. Four PDV probes were used to measure confiner velocity profiles at 2/3 of run distance. In the direction normal to detonation propagation, the probe position varied, with two located at the centerline (one probe on each side of assembly), one 10 mm offset from centerline, and the final probe 20 mm offset from centerline. Based on the (unconfined) slab tests in [2], the 2D flow at the breakout face of a PBX 9501 130$\times$150 mm slab will extend at least 20 mm on either side of the centerline (corresponding to a penetration angle of 22° for the 3D flow). This implies that the measurement sites, at 2/3 of the axial length, the 2D flow extends further still to $\approx$ 40 mm on either side of the centerline. Therefore, the chosen probe locations ensure the measured wall expansion is derived from a 2D flow in the HE. This key feature makes the computational comparisons described in section 4 tractable and meaningful.

The PDV traces for the cylinder test appear in Fig. 2 (left). The equivalent plot for the slab expansion tests appear in Fig. 3. As can be seen in the inset in each plot which isolates the late-time behavior, the data spread is around 20-30 m/s for both Cu-confined experiments. The probe records from the Ta test appear to show a more distinct separation but the overall range of velocities at a given time is similar (30 m/s). Given that the measured plate thicknesses at the probe sites were more variable (i.e. 0.544, 0.549 and 0.550 mm), a slightly increased probe-to-probe variation may be expected. Figure 4 (left) presents the front curvature record extracted from the CYLEX test and shows substantial curvature near the charge edges.

3 Numerical modeling and calibration

The wave propagation calculation within our PB method uses DSD to produce a time-of-arrival field ($t_b(\mathbf{x})$, with $\mathbf{x}$ being a point in the geometry). Figure 4 compares an unconfined DSD calculation using the propagation law in [2] and the recorded front shape for the CYLEX test. The similarity between the unconfined calculation and data suggests that the interaction was unconfined or nearly so. The small thickness of the intervening Sylgard 184 layer between HE and confiner (between 0.01 and 0.025 mm in

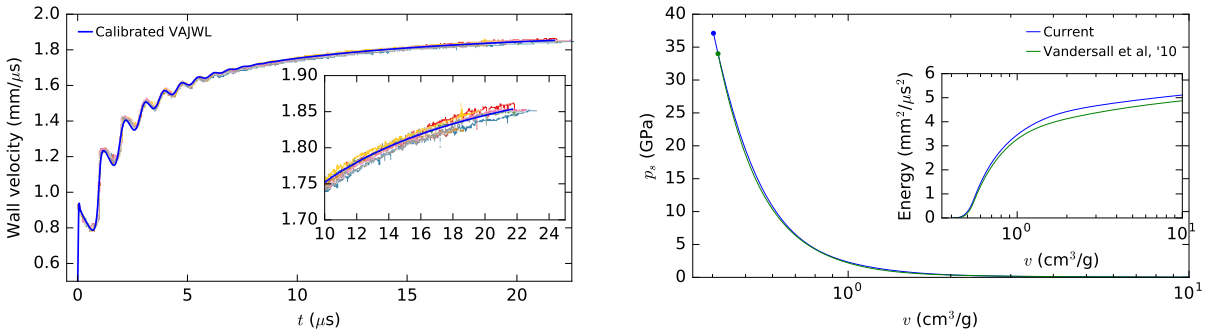

Figure 2: Left: The fitted wall motion (blue line) and comparison to data (in symbols). Right: The model pressure isentrope developed here.

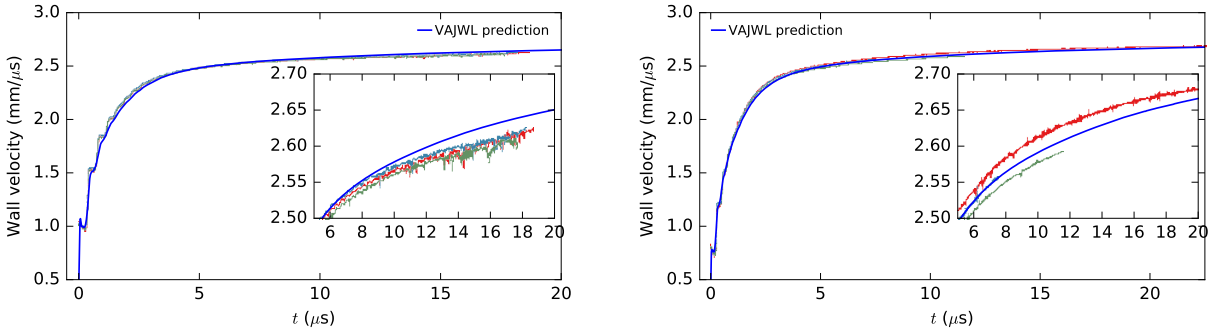

Figure 3: Left: The predicted wall motion (blue line) and comparison to the Cu slab test in symbols. Right: Same information for Ta slab.

thickness[2]) appears to generate an unconfined detonation propagation in the HE. However, the Sylgard layer has a negligible effect on the wall expansion itself given it is only about 0.07% of the total Cu mass.

To determine the energy release during the hydrodynamic phase of the calculation, the detonation velocity adjusted Jones-Wilkins-Lee (VAJWL) method is used. This is modification of the JWL equation-of-state [8], i.e.

$$p(v,e) = A\left(1 - \frac{\omega v_0}{R_1 v}\right)\exp\left(-\frac{R_1 v}{v_0}\right) + B\left(1 - \frac{\omega v_0}{R_2 v}\right)\exp\left(-\frac{R_2 v}{v_0}\right) + \frac{\omega}{v}(e - e' - E_{det}), \quad (1)$$

where p is pressure, e is the specific internal energy and v is specific volume and A, B, R_1, R_2, E_{det} and ω are the base model constants, $v_0 = 1/\rho_0$ and ρ_0 is the initial density and e' is a prescribed offset such that $p(v_0, 0) = 0$. For the VAJWL model, the JWL EOS is augmented with energy deposition offsets that depend on the local, spatially-dependent DSD front detonation velocity (D_n) and time of arrival (t_b) to achieve a measure of the finite-reaction zone effect (i.e. reduced pressure relative to CJ conditions).

Here, we use multi-material hydrodynamic simulations of the CYLEX test to constrain the parameters of the EOS parameters via an automated, iterative process (more detail is given in [3, 4, 5]). The confining copper material was modeled using a linear $U_s - U_p$ Mie-Grüneisen EOS model and a plastic deformation model described in [9]. Wall motion profiles at the outer copper surface at the experimentally-measured axial location are extracted from these simulations for comparison to experiment. The error

[2]These lengths are comparable or larger than the half reaction zone scale for PBX 9501 determined in [7]

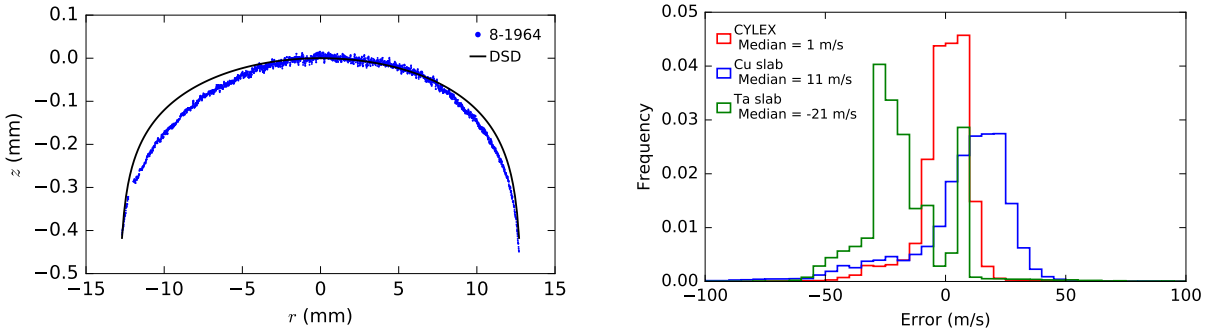

Figure 4: Left: DSD front calculation and record front shape. Right: Error distributions for fit and prediction calculations.

function incorporating this comparison is simply based on the average root-mean-square error for the multiple wall velocity measurements, similarly to [3, 4, 5]. The parameter set selected for optimization included A, B, R_1, R_2 and ω and the initial parameter set is based on the scaling-derived JWL from [10] which has been found to greatly accelerate the calibration process [3, 4, 5]. The parameter E_{det} is set at each calibration iteration such that the unperturbed EOS CJ velocity is consistent with the DSD CJ velocity parameter. A downhill simplex miniminization method [11] was used to numerical minimize the error function. After a convergence study for the wall motion profile, a resolution of 125 μm was selected to simulate the CYLEX test.

Table 2: The calibrated EOS parameters. The CJ state velocity, pressure and specific volume are 8.790 mm/μs, 37.11 GPa, and 0.4026 cm^3/g, respectively.

A (GPa)	B (GPa)	C (GPa)	R_1	R_2	ω	E_{det} (kJ/g)	ρ_0 (g/cm^3)
807.833	17.816	1.371	4.533	1.349	0.309	6.099	1.833

The numerical minimization of the defined merit function produces the parameters that appear in Table 2. Note that we have used the nominal density value for PBX 9501 to represent the explosive in the CYLEX test though as measured, the average density is marginally higher (1.837 g/cm^3). The fitted model calculation is compared to the data in Fig. 2 (left) showing the calculation lies within the spread of data due to the multiple measurement sites. The agreement is excellent. The optimized isentrope pressure appears in Fig. 2 (right). The isentrope for a JWL model [12] previously derived from cylinder and other metal plate acceleration data is also plotted for reference. This latter model isentrope possesses lower pressures at smaller volumes but this relationship eventually reverses for large enough volumes. The included inset also shows the corresponding integrated energy delivery for both models and confirms that the current model is significantly more energetic for the shown range.

4 Model validation

The two slab tests were modeled using the calibrated PB model and methods described in the preceding section. Like in the Cu case, the Ta material was modeled according to [9], however a higher resolution (62.5 μm) was used due to its much thinner thickness in the experiment. Figure 3 compares the predictions to the experimental traces, showing good agreement. How this agreement quantitatively compares to the fit error is detailed in Fig. 4 (right) which plots the accumulated fit and prediction error distributions for all three tests. This plot clarifies that the Cu slab test is slightly overestimated by our model,

mainly at late time. For the Ta slab, the error is more widespread due to the cited probe data separation and thus generally underestimates the experimental record, again, mainly at late time. This produces the larger peak at around -25 m/s in the Ta slab test error distribution. In terms of a single scalar error measure, the model generates 1, 11 and -21 m/s median errors for the Cu CYLEX, Cu slab and Ta slab tests, respectively. Relative to the late-time or maximum velocity, these measures represent less than a 0.8% error.

References

[1] J. B. Bdzil and D. S. Stewart. Modeling two-dimensional detonations with detonation shock dynamics. *Phys. Fluids A: Fluid Dyn.*, 1:1261, 1989.

[2] C. Chiquete, M. Short, E. K. Anderson, and S. I. Jackson. Detonation shock dynamics modeling and calibration of the HMX-based conventional high explosive PBX 9501 with application to the two-dimensional circular arc geometry. *Combust. Flame*, 222:213–232, 2020.

[3] C. Chiquete and S. I. Jackson. Detonation performance of the CL-20-based explosive LX-19. *Proc. Combust. Instit.*, 38(3):3661–3669, 2020. doi: https://doi.org/10.1016/j.proci.2020.07.089.

[4] C. Chiquete, S. I. Jackson, E. K. Anderson, and M. Short. Detonation performance experiments and modeling for the DAAF-based high explosive PBX 9701. *Combust. Flame*, 223:382–397, 2020. doi: https://doi.org/10.1016/j.combustflame.2020.10.009.

[5] E. K. Anderson, C. Chiquete, S. I. Jackson, R. I. Chicas, and M. Short. The comparative effect of HMX content on the detonation performance characterization of PBX 9012 and PBX 9501 high explosives. *Combust. Flame*, 230:111415, 2021.

[6] M. A. Zocher, T. D. Aslam, S. I. Jackson, and E. K. Anderson. Numerical modeling comparing slab to cylinder test expansion geometries for PBX 9501. In *Proc. 16th Intl. Det. Symp.*, pages 1137–1147. Office of Naval Research, 2018.

[7] M. Short, E. K. Anderson, C. Chiquete, and S. I. Jackson. Experimental and modeling analysis of detonation in circular arcs of the conventional high explosive PBX 9501. *Proc. Combust. Instit.*, 38(3):3683–3690, 2020. doi: https://doi.org/10.1016/j.proci.2020.07.107.

[8] E. Lee, M. Finger, and W. Collins. JWL equation of state coefficients for high explosives. Technical Report UCID-16189, Lawrence Livermore National Laboratory, 1973.

[9] D. L. Preston, D. L. Tonks, and D. C. Wallace. Model of plastic deformation for extreme loading conditions. *J. Appl. Phys.*, 93(1):211–220, 2003.

[10] S. I. Jackson. Scaling of the detonation product state with reactant kinetic energy. *Combust. Flame*, 190:240–251, 2018.

[11] J. A. Nelder and R. Mead. A simplex method for function minimization. *The Comp. J.*, 7(4): 308–313, 1965.

[12] K. S. Vandersall, C. M. Tarver, F. Garcia, and S. K. Chidester. On the low pressure shock initiation of octahydro-1, 3, 5, 7–tetranitro-1, 3, 5, 7-tetrazocine based plastic bonded explosives. *J. Appl. Phys.*, 107(9):094906, 2010.